PAPR Suppression Method for Probability-oriented MP-WFRFT

Yuxiao Yang, Xiaolu Zhang, and Xiaobo Shen

***Abstract*—The peak-to-average power ratio (PAPR) suppression method typically leads to the deterioration of bit error rate (BER) performance. The multi-parameter weighted fractional Fourier transform (MP-WFRFT) can suppress the PAPR by adjusting the proportion of its single-carrier and multi-carrier components. Due to the unitary matrix characteristics of MP-WFRFT, the system BER remains unaffected. Additionally, due to its hybrid carrier characteristics, MP-WFRFT also exhibits excellent anti-scanning capability. The MP-WFRFT can enhance the security performance of communication signals by reconstructing their modulation constellation diagrams. This paper introduces a mathematical model for control variables and PAPR effect mechanism of MP-WFRFT for the first time by using intermediate analysis variables such as single-carrier weight factor and multi-carrier weight factor. The simulation results indicate that the proposed method can significantly reduce the PAPR of the system without affecting the BER.**

***Index Terms*—MP-WFRFT, probability density function (PDF), PAPR, complementary cumulative distribution function (CCDF).**

I. Introduction

MULTI-CARRIER (MC) modulation can effectively resist multipath fading and intersymbol interference during communication, so it has been widely applied in 5G and UAV communications. However, the primary disadvantage of MC modulation lies in its high PAPR, which adversely impacts the system's BER performance.

Over the years, three primary PAPR suppression methods for MC modulation have been developed: probability method [1], encoding method [2] and pre-distortion method. Probability and encoding methods have high computational complexity and present challenges in the resource-constrained system. The pre-distortion method is the most widely applied PAPR suppression at present [3]–[5], but nonlinear operation will cause signal distortion and BER deterioration. Therefore, to solve the BER deterioration is the key of pre-distortion method.

MP-WFRFT is a typical hybrid carrier system capable of controlling PAPR by adjusting the proportion of single-carrier (SC) components and MC components. As the MP-WFRFT matrix is a unitary matrix, it is less affected by noise power and will not cause BER deterioration [6]. Therefore, MP-WFRFT method can solve such a problem that the optimal performances of PAPR and BER cannot be simultaneously achieved by traditional pre-distortion methods. The proposed method has an important application potential.

MP-WFRFT employs 9 control variables (including transformation order and scale vector), enabling flexible waveform design and complex constellation mapping by adjusting these variables. Currently, the primary research focus for MP-WFRFT is on the reconstruction design of the constellation diagram. For the security of communication signals, Reference [7] further analyzed the mechanism between the control parameters of MP-WFRFT and the scaling, rotation and splitting of the signal modulation constellation, proposing a secure communication system design method based on WFRFT-TDCS. This proposed method achieves better anti-interception performance, which shows that the constellation reconstruction capability of MP-WFRFT can help improve the security performance of the communication system. References [8] and [9] proposed a new constellation superposition mathematical model for the constellation diagram reconstruction problem of communication signals. The model provides the quantitative analysis constraints of constellation ambiguity and fission, realizing the reconstruction deception design of familiar signal constellations such as QPSK and 8PSK, and verifying the feasibility of the MP-WFRFT constellation deception method. Reference [10] combined artificial noise and chaotic scrambling with MP-WFRFT under the advantages of constellation deception. It proposed a new secure communication method, effectively improving the power efficiency and security performance of wireless transmission, and indicating that MP-WFRFT has good system scalability.

However, MP-WFRFT has numerous control parameters including 9 control variables [11], making the effect mechanism between control variables and PAPR rather complicated. At present, there is no study on the PAPR effect mechanism of MP-WFRFT. Single-parameter weighted fractional Fourier transform (SP-WFRFT) only involves transform order (a control variable), so the effect mechanism between control variables and PAPR performance is clear. There are only a few studies on the PAPR of SP-WFRFT. Reference [12] combined SP-WFRFT with traditional PAPR optimization method (CAF) to obtain better PAPR and BER performances, which indicated that WFRFT was beneficial to the optimization of PAPR. References [13] and [14] adopted the PDF of signal as an analysis tool to theoretically interpret the relationship between the transform order of SP-WFRFT and PAPR. However, MP-WFRFT has far more control variables than SP-WFRFT, so the PAPR analysis method of the SP-WFRFT system cannot be directly applied to MP-WFRFT. In view of this, to study the PAPR analysis methods for MP-WFRFT is urgently required.

In this work, we have designed the hybrid carrier system of

Manuscript received June 17, 2024; revised October 17, 2024.

Yuxiao Yang is a professor of Nanjing University of Aeronautics and Astronautics, Nanjing, 210000 China. (phone: 025-84896859; fax: 025-84896112; e-mail: yyx_ nuaa@163.com).

Xiaolu Zhang is a postgraduate student of Nanjing University of Aeronautics and Astronautics, Nanjing, 210000 China. (e-mail: zxlu98@nuaa.edu.cn).

Xiaobo Shen is a postgraduate student of Nanjing University of Aeronautics and Astronautics, Nanjing, 210000 China. (e-mail: shenxiaobo@nuaa.edu.cn).

MP-WFRFT based on probability. The main contributions of this work are as follows: In this paper, the effect mechanism between control variables and PAPR performance of MP-WFRFT is provided mathematically for the first time. The mathematical expression of the PDF of MP-WFRFT is deduced by taking SC weight factor and MC weight factor as intermediate analysis variables and classification conditions. Then, PDF serves as a mathematical bridge to provide the mathematical expression for the CCDF of MP-WFRFT. Due to the unitary matrix characteristics of MP-WFRFT, no BER performance loss is caused.

II. PRELIMINARIES

In this chapter, we introduce a four MP-WFRFT model, which is a linear weighted superposition of Fourier functions in different states. The MP-WFRFT of any complex sequence $X_0(n)$ can be expressed as:

$$S(n)=\sum_{\ell=0}^{3}\omega_\ell(\alpha,\mathbf{V})X_\ell(n) \tag{1}$$

Where $X_\ell(n)$ is the ℓth DFT transform of $X_0(n)$, and $\omega_\ell(\alpha,\mathbf{V})$ is the weighting coefficient.

For MP-WFRFT, $\omega_\ell(\alpha,\mathbf{V})$ is expressed as:

$$\begin{aligned}&\omega_\ell(\alpha,\mathbf{V})=\\&\frac{1}{4}\sum_{\mathrm{k}=0}^{3}\exp\left\{\pm\frac{2\pi j}{4}\left[\left(4m_k+1\right)\alpha\left(k+4n_k\right)-\ell k\right]\right\}=\\&\frac{1}{4}\left[\exp\left(\lambda_0\right)+(-j)^l\exp\left(\lambda_1\right)+\right.\\&\quad\left.(-1)^l\exp\left(\lambda_2\right)+(j)^l\exp\left(\lambda_3\right)\right],\ell=0,1,2,3\end{aligned} \tag{2}$$

Where α is the transform order, $\mathbf{V}$ is the scale vector, $\mathbf{V}=[m_0,m_1,m_2,m_3,n_0,n_1,n_2,n_3]$, and $\lambda_k=\frac{2\pi j}{4}(4m_k+1)\alpha(k+4n_k)$.

The SC and MC characteristics of MP-WFRFT can be measured by SC weight factor W_{sc} and MC weight factor W_{mc}. W_{sc} and W_{mc} are shown in the following equation:

$$\begin{cases}W_{sc}=\left|\omega_0(\alpha,\mathbf{V})\right|^2+\left|\omega_2(\alpha,\mathbf{V})\right|^2\\W_{mc}=\left|\omega_1(\alpha,\mathbf{V})\right|^2+\left|\omega_3(\alpha,\mathbf{V})\right|^2\end{cases} \tag{3}$$

According to Equation (2), we can obtain:

$$\sum_{\ell=0}^{3}\left|\omega_\ell(\alpha,\mathbf{V})\right|^2=W_{sc}+W_{mc}=1 \tag{4}$$

Suppose that WFRFT matrix is $\mathbf{W}$. As WFRFT is a unitary matrix (non-singular matrix), then:

$$\mathbf{W}^H\mathbf{W}=\mathbf{W}\mathbf{W}^H=\mathbf{E} \tag{5}$$

Therefore, WFRFT signal can retain noise covariance, and the signal BER is less affected by noise.

Additionally, MP-WFRFT exhibits excellent signal anti-scanning capability. α and $\mathbf{V}$ control the scaling, rotation, and splitting of the signal modulation constellation. When the condition $W_{sc}\neq 1, W_{mc}\neq 0$ is met, the hybrid carrier signal displays Gaussian statistical properties in both time and frequency domains. For the widely applied blind signal detection methods based on higher-order cumulants, the higher-order cumulants of Gaussian signals are always zero. This state significantly increases the difficulty for the interceptor to conduct blind detection. Moreover, the MP-WFRFT system primarily processes communication signals in the WFRFT transform domain, which effectively adds physical layer encryption to the original communication signal. The MP-WFRFT transformation matrix $\mathbf{W}_{\alpha,\mathbf{V}}$ plays a crucial role in controlling the scaling, rotation, and splitting of the signal modulation constellation, enabling the constellation deception of the communication signal. $\omega_1(\alpha,\mathbf{V})X_1(n)$ and $\omega_3(\alpha,\mathbf{V})X_3(n)$, the frequency-domain components in the hybrid carrier, determine the Gaussian fuzzy characteristics of the constellation diagram through their synthesis. $\omega_0(\alpha,\mathbf{V})X_0(n)$ and $\omega_2(\alpha,\mathbf{V})X_2(n)$, the time-domain components in the hybrid carrier, determine the fission characteristics of the constellation diagram. As shown in Fig.1, the original signal constellation diagram can undergo specific fuzzy and splitting changes by utilizing a specially optimized transformation matrix $\mathbf{W}_{\alpha,\mathbf{V}}$, generating a new constellation diagram with entirely different modulation characteristics. This approach deceives the interception process of the malicious interceptor, enhancing the security capability of the communication system. If the interceptor does not obtain all the MP-WFRFT control parameters, it will be difficult to correctly demodulate the communication signal, significantly enhancing the security of the communication system.

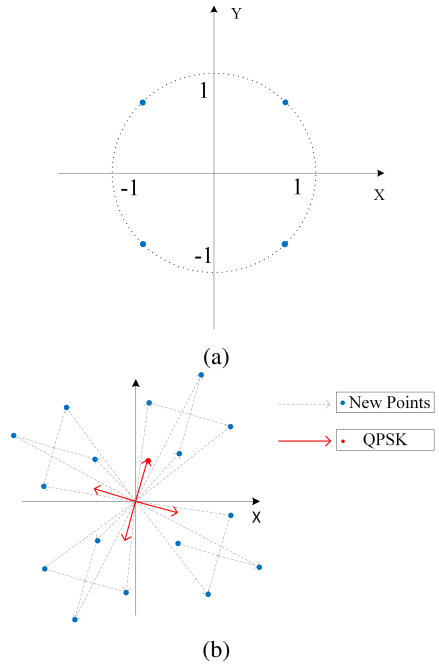

Fig. 1: Original QPSK constellation and 16QAM deception constellation.

III. THE PROPOSED METHOD

In this chapter, we provide a mathematical relationship between the control variables and the PAPR performance of MP-WFRFT. The system block diagram of PAPR suppression mechanisms is shown in Fig. 2.

A. PDF Deduction Based on Weight Factors

The essence of the suppression of PAPR by MP-WFRFT is to change the energy distribution of SC and MC components,

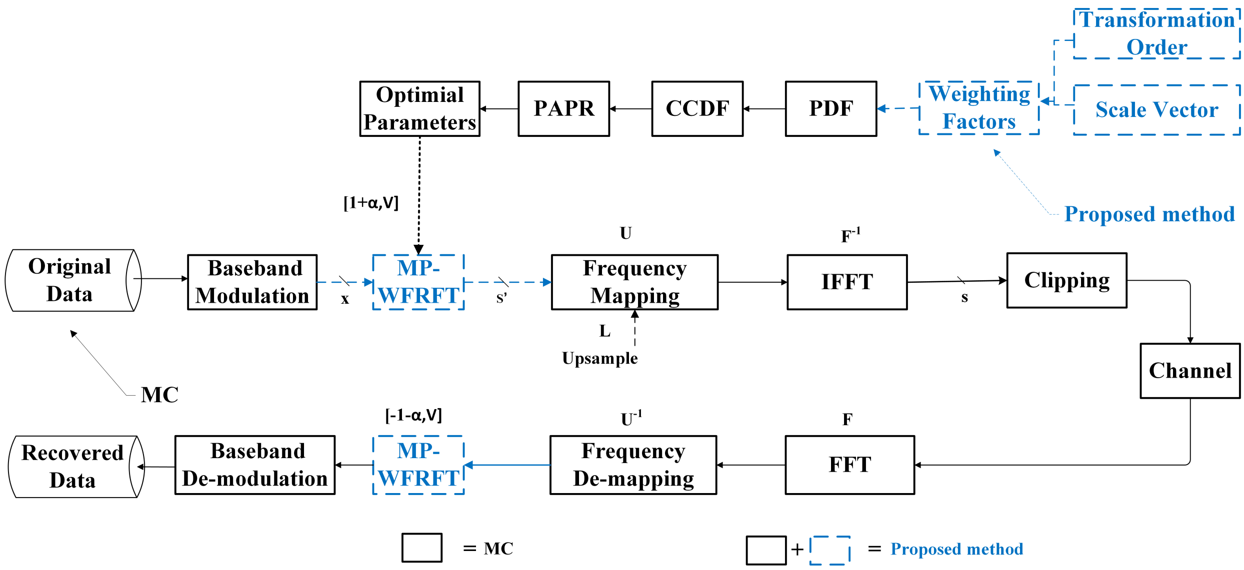

Fig. 2: Framework of hybrid carrier system in PAPR suppression mechanisms.

which is be characterized by PDF. In this section, PDF is deduced for the orthogonal component of s in Fig. 2, and QPSK is used for baseband mapping. According to the additivity of Equation (1) and the matrix of MP-WFRFT, the orthogonal component of $s(n)$ is as follows:

$$\Re e[\mathrm{s}(n)] = \sum_{l=0}^{3} \Re e\left[\omega_l(\alpha, \mathbf{V}) X_l(n)\right] = \sum_{l=0}^{3} \Re e \left[\frac{1}{4}\sum_{k-0}^{3} \exp\left[\pm\frac{2\pi j}{4}[(4m_k+1)\alpha(k+4n_k) - \ell k]\right] X_\ell(n)\right] \tag{6}$$

Thus, the PDF of $\Re e[s(n)]$ is a function of α and $\mathbf{V}$, 9 control parameters are independent of each other, and it is difficult to directly analyze the variation law of PDF through these nine parameters. Therefore, we need to design an intermediate variable determined by α and $\mathbf{V}$ so as to analyze PDF. The weight factors (W_{sc} and W_{mc}) are taken as intermediate variables to analyze the PDF of MP-WFRFT. The following two cases ($W_{sc} = 1, W_{mc} = 0$ and $W_{sc} \neq 1, W_{mc} \neq 0$) are discussed.

1) $W_{sc} = 1, W_{mc} = 0$: In this case, the following equation can be obtained according to Equation (3):

$$\omega_1(\alpha, \mathbf{V}) = \omega_3(\alpha, \mathbf{V}) = 0 \tag{7}$$

According to Equations (2) and (7), the relationship equation of λ_k can be obtained:

$$\exp(\lambda_0) = \exp(\lambda_2), \exp(\lambda_1) = \exp(\lambda_3) \tag{8}$$

Then:

$$\omega_0(\alpha, \mathbf{V}) + \omega_2(\alpha, \mathbf{V}) = \exp(\lambda_0) = 1 \tag{9}$$

Due to $W_{sc} = |\omega_0(\alpha, \mathbf{V})|^2 + |\omega_2(\alpha, \mathbf{V})|^2 = 1$, then $\omega_0(\alpha, \mathbf{V}) = 1, \omega_2(\alpha, \mathbf{V}) = 0$ or $\omega_0(\alpha, \mathbf{V}) = 0, \omega_2(\alpha, \mathbf{V}) = 1$.

After $\omega_\ell(\alpha, \mathbf{V}), \ell = 0, 1, 2, 3$ is substituted into Equation (6), $\Re e[\mathrm{s}(n)] = \Re e\left[X_0(n)\right]$ or $\Re e[\mathrm{s}(n)] = \Re e\left[X_2(n)\right]$ where $X_2(n)$ is the time domain reverse signal of $X_0(n)$. For QPSK, $Pr\{\Re e[s(n)] = \pm 1\} = \frac{1}{2}$. Similarly, $Pr\{\Im m[s(n)] = \pm 1\} = \frac{1}{2}$. When $W_{sc} = 1, W_{mc} = 0$, MP-WFRFT is in a SC state, $\Re e[\mathrm{s}(n)]$ and $\Im m[s(n)]$ follow the Bernoulli distribution.

2) $W_{sc} \neq 1, W_{mc} \neq 0$: In this case, MP-WFRFT is in a hybrid carrier state, and the distribution of $\Re e[\mathrm{s}(n)]$ can be obtained by analyzing the distribution of the four components in Equation (6).

a) $\Re e[\omega_0(\alpha, \mathbf{V}) X_0(n)]$ and $\Re e[\omega_2(\alpha, \mathbf{V}) X_2(n)]$: $\Re e[\omega_0(\alpha, \mathbf{V}) X_0(n)]$ can be expressed as:

$$\Re e\left[\omega_0(\alpha, \mathbf{V}) X_0(n)\right] = \Re e\left[\omega_0(\alpha, \mathbf{V}) \cdot \left((-1)^{k_1} + \mathrm{j} \cdot (-1)^{k_2}\right)\right], \mathrm{k}_1, \mathrm{k}_2 \in \{0, 1\} \tag{10}$$

According to Equation (2), $\omega_0(\alpha, \mathbf{V})$ is expanded with Euler's Formula to obtain the following expression:

$$\begin{aligned} \omega_0(\alpha, V) &= \frac{1}{4}\sum_{k=0}^{3} \exp\left(\frac{2\pi j}{4}\alpha(4m_k+1)(k+4n_k)\right) \\ &= \frac{1}{4}\sum_{k=0}^{3} [\cos\left(\frac{\pi}{2}\alpha(4m_k+1)(k+4n_k)\right) + \\ &\quad j\sin\left(\frac{\pi}{2}\alpha(4m_k+1)(k+4n_k)\right)] \end{aligned} \tag{11}$$

According to Equations (10) and (11), $\Re e[\omega_0(\alpha, \mathbf{V}) X_0(n)]$ has four values $A_i (i = 0, 1, 2, 3)$ which are specifically expressed as:

$$\left\{\begin{aligned} &A_0 = -A_2 = \\ &\tfrac{1}{4}\sum_{k=0}^{3}\left[\cos\left(\tfrac{\pi}{2}\alpha\left(4m_k+1\right)\left(k+4n_k\right)\right) - \right. \\ &\qquad\left.\sin\left(\tfrac{\pi}{2}\alpha\left(4m_k+1\right)\left(k+4n_k\right)\right)\right] \\ &A_1 = -A_3 = \\ &\tfrac{1}{4}\sum_{k=0}^{3}\left[\cos\left(\tfrac{\pi}{2}\alpha\left(4m_k+1\right)\left(k+4n_k\right)\right) + \right. \\ &\qquad\left.\sin\left(\tfrac{\pi}{2}\alpha\left(4m_k+1\right)\left(k+4n_k\right)\right)\right] \end{aligned}\right. \tag{12}$$

Therefore, $\Re e[\omega_0(\alpha, \mathbf{V}) X_0(n)]$ satisfies the discrete and uniform distribution. As $X_2(n)$ is the time domain reverse signal of $X_0(n)$, $\Re e[\omega_2(\alpha, \mathbf{V}) X_2(n)]$ also satisfies the discrete and uniform distribution, and the value set is $B_j (j = 0, 1, 2, 3)$, as shown in Equation (13).

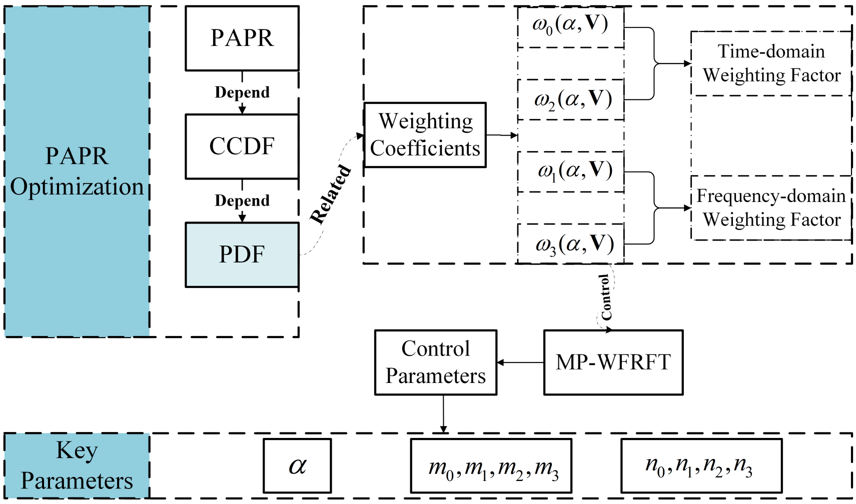

Fig. 3: PAPR compression mechanism of MP-WFRFT.

$$\begin{cases} B_0 = -B_2 = \\ \frac{1}{4}\sum_{k=0}^{3}\left\{\cos\left[\frac{\pi}{2}\left(\alpha\left(4m_k+1\right)\left(k+4n_k\right)-2k\right)\right] - \right. \\ \left. \qquad \sin\left[\frac{\pi}{2}\left(\alpha\left(4m_k+1\right)\left(k+4n_k\right)-2k\right)\right]\right\} \\ B_1 = -B_3 = \\ \frac{1}{4}\sum_{k=0}^{3}\cos\left[\frac{\pi}{2}\left(\alpha\left(4m_k+1\right)\left(k+4n_k\right)-2k\right)\right] + \\ \qquad \sin\left[\frac{\pi}{2}\left(\alpha\left(4m_k+1\right)\left(k+4n_k\right)-2k\right)\right] \end{cases} \tag{13}$$

b) $\Re e[\omega_1(\alpha,\mathbf{V})X_1(n)]$ and $\Re e[\omega_3(\alpha,\mathbf{V})X_3(n)]$: When the number of subcarriers is large, it can be found from the central limit theorem that $\Im m[X_1(n)]$ and $\Re e[X_1(n)]$ follow the Gaussian distribution and are independent of each other. Then, $\Re e[\omega_1(\alpha,\mathbf{V})X_1(n)]$ can be expressed as:

$$\begin{aligned} &\Re e\left[\omega_1(\alpha,\mathbf{V})X_1(n)\right] = \\ &\Re e[\omega_1(\alpha,\mathbf{V})]\Re e[X_1(n)] - \Im m[\omega_1(\alpha,\mathbf{V})]\Im m[X_1(n)] \end{aligned} \tag{14}$$

As $\Re e[\omega_1(\alpha,\mathbf{V})]\Re e[X_1(n)]$ and $\Im m[\omega_1(\alpha,\mathbf{V})]\Im m[X_1(n)]$ are independent Gaussian variables, their linear combination will also satisfy $\Re e[\omega_1(\alpha,\mathbf{V})X_1(n)] \sim N(0,\sigma_1^2(\alpha,\mathbf{V}))$. Similarly, $\Re e[\omega_3(\alpha,\mathbf{V})X_3(n)] \sim N(0,\sigma_3^2(\alpha,\mathbf{V}))$. According to Equation (3), we can obtain:

$$\Re e\left[\omega_1(\alpha,\mathbf{V})X_1(n)\right] + \Re e\left[\omega_3(\alpha,\mathbf{V})X_3(n)\right] \sim N(0,W_{mc}) \tag{15}$$

c) Distribution of $\Re e[s(n)]$ and PDF deduction.

As $\Re e\left[\omega_1(\alpha,\mathbf{V})X_1(n)\right] + \Re e\left[\omega_3(\alpha,\mathbf{V})X_3(n)\right]$ satisfy the Gaussian distribution of $N(0,W_{mc})$, and they are independent of $\Re e\left[\omega_0(\alpha,\mathbf{V})X_0(n)\right]$ and $\Re e\left[\omega_2(\alpha,\mathbf{V})X_2(n)\right]$. The intermediate variable u is defined as:

$$\begin{aligned} u &= \Re e\left[\omega_0(\alpha,\mathbf{V})X_0(n)\right] + \\ &\Re e\left[\omega_1(\alpha,\mathbf{V})X_1(n)\right] + \Re e\left[\omega_3(\alpha,\mathbf{V})X_3(n)\right] \end{aligned} \tag{16}$$

Considering u complies with the Gaussian distribution, the PDF $f(u)$ of the variable can be expressed as:

$$\begin{aligned} f(u) &= \frac{dF(u)}{du} \\ &= \left(\sum_{i=0}^{3}\frac{1}{4}\cdot \Pr\{\Re e\left[\omega_1(\alpha,\mathbf{V})X_1(n)\right]\right. \\ &\quad \left. + \Re e\left[\omega_3(\alpha,\mathbf{V})X_3(n)\right] \leqslant u - \mathrm{A}_i\}\right)' \\ &= \left(\sum_{i=0}^{3}\frac{1}{4}\cdot F(u-\mathrm{A}_i)\right)' = \sum_{i=0}^{3}\frac{1}{4}f(u-\mathrm{A}_i) \\ &= \sum_{i=0}^{3}\frac{1}{4\sqrt{2\pi W_{mc}}}e^{-\frac{(u-\mathrm{A}_i)^2}{2W_{mc}}}, -\infty < u < +\infty \end{aligned} \tag{17}$$

Suppose $v = \Re e[s(n)] = u + \Re e[\omega_2(\alpha,V)X_2(n)]$. As u is independent of $\Re e\left[\omega_2(\alpha,\mathbf{V})X_2(n)\right]$, $f(v)$ is as follows:

$$\begin{aligned} f(v) &= \left(\Pr\{u + \Re e\left[\omega_2(\alpha,V)X_2(n)\right] \le v\}\right)' \\ &= \left(\sum_{j=0}^{3}\frac{1}{4}\cdot \Pr\{u \le u - B_j\}\right)' = \sum_{j=0}^{3}\frac{1}{4}\cdot f(u-B_j) \\ &= \sum_{i=0}^{3}\sum_{j=0}^{3}\frac{1}{16\sqrt{2\pi W_{mc}}}e^{-\frac{(v-A_i-B_j)^2}{2W_{mc}}}, -\infty < 0 < +\infty \end{aligned} \tag{18}$$

Therefore, the PDF expression of MP-WFRFT is as follows:

$$f(v) = \begin{cases} \frac{1}{2}\delta(v+1) + \frac{1}{2}\delta(v-1), \\ v \in \mathbb{R}\,(W_{sc}=1, W_{mc}=0) \\ \sum_{i=0}^{3}\sum_{\mathrm{j}=0}^{3}\frac{1}{16\sqrt{2\pi W_{mc}}}e^{-\frac{(v-A_i-B_j)^2}{2W_{mc}}}, \\ v \in \mathbb{R}\,(W_{sc}\neq 1, W_{mc}\neq 0) \end{cases} \tag{19}$$

After comparing the PDF expression (19) with the Gaussian PDF expression [15], $f(\Re e[\mathrm{s}(n)])$ can be expressed as the superposition of 16 Gaussian PDFs which satisfy $N(A_i+B_j, W_{mc})$, $i,j \in \{0,1,2,3\}$.

B. PAPR Deduction of MP-WFRFT Based on PDF

Assuming that the powers of the in-phase component and orthogonal component of $s(n)$ are $P_{\mathrm{i}}^{\alpha,\mathbf{V}}$ and $P_{\mathrm{q}}^{\alpha,\mathbf{V}}$ respectively, the power of MP-WFRFT is $P_{HC}^{\alpha,\mathbf{V}}$, and the CDF of $P_{HC}^{\alpha,\mathbf{V}}$ can be expressed as:

$$\begin{aligned}
&F\left(P_{HC}^{\alpha,\mathbf{V}}\right)=\Pr\left(P_{\mathrm{i}}^{\alpha,\mathbf{V}}+P_{q}^{\alpha,\mathbf{V}}\leq P_{HC}^{\alpha,\mathbf{V}}\right)\\
&=\iint_{P_{i}^{\alpha,\mathbf{V}}+P_{q}^{\alpha,\mathbf{V}}\leq P_{HC}^{\alpha,\mathbf{V}}} f\left(P_{\mathrm{i}}^{\alpha,\mathbf{V}}\right)\cdot f\left(P_{q}^{\alpha,\mathbf{V}}\right)dP_{q}^{\alpha,\mathbf{V}}dP_{\mathrm{i}}^{\alpha,\mathbf{V}}\\
&=\int_{0}^{P_{HC}^{\alpha,\mathbf{V}}}\int_{0}^{P_{HC}^{\alpha,\mathbf{V}}-P_{q}^{\alpha,\mathbf{V}}} f\left(P_{\mathrm{i}}^{\alpha,\mathbf{V}}\right)\cdot f\left(P_{q}^{\alpha,\mathbf{V}}\right)dP_{q}^{\alpha,\mathbf{V}}dP_{\mathrm{i}}^{\alpha,\mathbf{V}}
\end{aligned} \tag{20}$$

Where $f\left({P_{\mathrm{i}}}^{\alpha,\mathbf{V}}\right)$ and $f\left({P_{\mathrm{q}}}^{\alpha,\mathbf{V}}\right)$ are the PDFs of ${P_{\mathrm{i}}}^{\alpha,\mathbf{V}}$ and ${P_{\mathrm{q}}}^{\alpha,\mathbf{V}}$, and their definitions are given in (19).

As the distribution function and density of the maximum value in the sample can be obtained by the order statistics arranged in an ascending order, the PDF of the maximum instantaneous power is as follows according to the principle of maximum order statistics:

$$f_{P_{HCm}^{\alpha,\mathbf{V}}}(P_{HC}^{\alpha,\mathbf{V}})=\mathrm{N}\cdot F'\left(P_{HC}^{\alpha,\mathbf{V}}\right)\cdot\left[F\left(P_{HC}^{\alpha,\mathbf{V}}\right)\right]^{N-1} \tag{21}$$

The CDF of the maximum instantaneous power of $P_{HC}^{\alpha,\mathbf{V}}$ is as follows:

$$F_{P_{HCm}^{\alpha,\mathbf{V}}}\left(P_{HC}^{\alpha,\mathbf{V}}\right)=\left[F\left(P_{HC}^{\alpha,\mathbf{V}}\right)\right]^{N} \tag{22}$$

The CCDF of $s(n)$ is expressed as:

$$\begin{aligned}
CCDF_{PAPR}(PAPR_0)&=1-F_{P_{HCm}^{\alpha,\mathbf{V}}}(PAPR_0\cdot P_{ave}^{\alpha,\mathbf{V}})\\
&=1\text{-}\left[F\left(PAPR_0\cdot P_{ave}^{\alpha,\mathbf{V}}\right)\right]^{N}
\end{aligned} \tag{23}$$

Where $P_{ave}^{\alpha,\mathbf{V}}$ denotes the average signal power when the parameter of MP-WFRFT is $[\alpha,\mathbf{V}]$, and $PAPR_0$ denotes the set threshold.

The PAPR compression mechanism of MP-WFRFT-CNC is shown in Fig. 3. After using genetic algorithms in (24), the following optimal parameter sets with the best PAPR performance can be obtained: α=1.1849, $\mathbf{V}=[4,2,7,2,7,8,5,6]$.

IV. SIMULATION AND ANALYSIS

In this chapter, we conduct a simulation experiment to compare the PAPR and BER performances of the proposed method with two traditional methods. The simulation parameters are as follows: The number (N) of sub-channels is 128, the number of symbols is 1,000, and the threshold $PAPR_0$ is 6.5dB (CCDF=10^{-3}).

A. PAPR Performance Comparison

The CCDF curves of the proposed method and the two traditional methods are shown in Fig. 4, in which the number of iterations of the ICF method is set as 3. The simulation results indicate that the proposed method has the optimal PAPR suppression, which is better than MC-Clipping and MC-ICF at the same clipping rate. In case of CCDF=10^{-3}, PAPR reaches a threshold value of 7.7dB in the proposed method.

B. BER Performance Comparison

The BER curves of the proposed method and the two traditional methods are shown in Fig. 5. The simulation results show that MC-Clipping and MC-ICF methods cause the deterioration of the system BER and the performance loss of 0.9 dB-2.0 dB. As the WFRFT matrix is a unitary matrix, MP-WFRFT is less affected by noise power. Therefore, the proposed method do not deteriorate the BER. Even at a high SNR, the WFRFT unitary transform can recover the data symbols accurately, which optimizes the BER performance to some extent.

C. Anti-scanning Performance Comparison

The nine parameters of MP-WFRFT are crucial for achieving anti-interception performance. If the interceptor does not obtain all the MP-WFRFT control parameters, it will be difficult to achieve correct demodulation of communication signals. Therefore, the most critical control parameter affecting the anti-scanning performance of the signal is the MP-WFRFT's parameter set $[\alpha,\mathbf{V}]$.

The control parameters of MP-WFRFT comprise nine variables, including transform order and scale vector. This section describes three scenarios in which a malicious interceptor may obtain MP-WFRFT control parameters to address potential key leakage resulting from parameter scanning. These scenarios include: 1. Missing transform order or scale vector control parameters; 2. Completely grasping the scale vector parameters but having errors in the transform order parameters; 3. Completely grasping the transform order parameters but having errors in the scale vector parameters. The control parameter settings for these three scenarios are shown in Table I. This section conducts the simulation analysis to evaluate the anti-scanning performance of the parameters in the above three scenarios.

$$\begin{cases}
\min G(\alpha,\mathbf{V},\gamma,\mu)=\sqrt{\left(\omega_0(1+\alpha,\mathbf{V})-r\times\omega_2(1+\alpha,\mathbf{V})\right)^2}+\sqrt{\left(PAPR-PAPR_0\right)^2}\\
s.t.\quad \alpha\in[0,4)\in\mathbb{R},\mathbf{V}=[\mathfrak{M},\mathfrak{N}];\mathfrak{M}=[m_0,m_1,m_2,m_3]\in\mathbb{Z}^4;\mathfrak{N}=[n_0,n_1,n_2,n_3]\in\mathbb{Z}^4;\\
\qquad m_k,n_k\in[0,10],k=0,1,2,3;\\
\qquad \omega_\ell(\alpha,\mathbf{V})=\dfrac{1}{4}\displaystyle\sum_{\mathrm{k}=0}^{3}\exp\left\{\pm\dfrac{2\pi j}{4}[(4m_k+1)\alpha(k+4n_k)-\ell k]\right\},\ell=0,1,2,3;\\
\qquad CCDF_{PAPR}(PAPR_0)=\Pr\left(PAPR>PAPR_0\right),CCDF=10^{-3},PAPR_0=6\mathrm{d}B;\\
\qquad \gamma\in\mathbb{R},\mu\in(0,8]\in N^{+};
\end{cases} \tag{24}$$

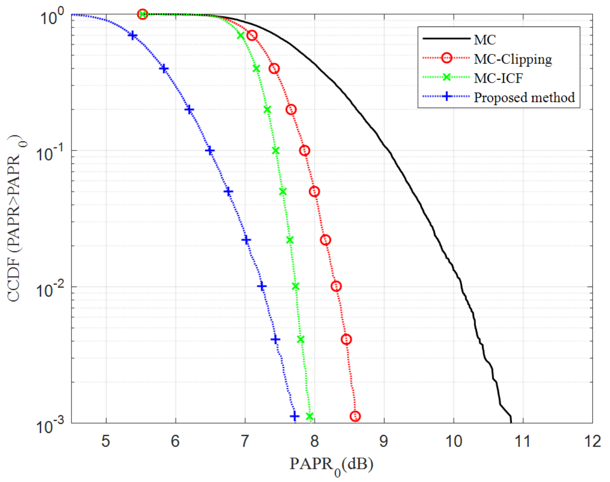

Fig. 4: PAPR performance comparison.

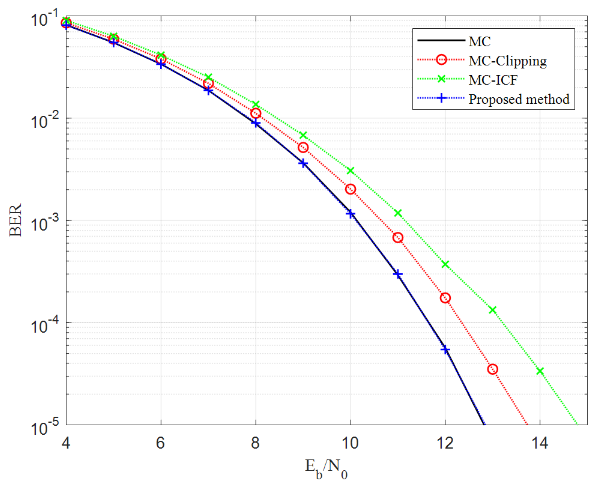

Fig. 5: BER performance comparison.

TABLE I: Signal Parameters In Different Scenarios

Scenarios	Transmitter α	Parameter m	Settings n	Illegal Receiver
	0.0000	[4,2,7,2]	[7,8,5,6]	Unknownα
1)	1.1849	[0,0,0,0]	[0,0,0,0]	Unknown$\mathbf{V}$
	0.0000	[0,0,0,0]	[0,0,0,0]	Unknownα, $\mathbf{V}$
	1.1949			$\Delta\alpha = 0.01$
2)	1.1859	[4,2,7,2]	[7,8,5,6]	$\Delta\alpha = 0.001$
	1.1850			$\Delta\alpha = 0.0001$
		[4,2,8,2]		$\kappa = 1, \Delta\mathbf{V} = 1$
		[4,2,9,2]	[7,8,5,6]	$\kappa = 1, \Delta\mathbf{V} = 2$
		[4,2,10,2]		$\kappa = 1, \Delta\mathbf{V} = 3$
		[4,3,8,2]		$\kappa = 2, \Delta\mathbf{V} = 1$
3)	1.1849	[4,4,9,2]	[7,8,5,6]	$\kappa = 2, \Delta\mathbf{V} = 2$
		[4,5,10,2]		$\kappa = 2, \Delta\mathbf{V} = 3$
		[5,3,7,2]	[4,2,8,2]	$\kappa = 3, \Delta\mathbf{V} = 1$
		[6,4,7,2]	[4,2,9,2]	$\kappa = 3, \Delta\mathbf{V} = 2$
		[7,5,7,2]	[4,2,10,2]	$\kappa = 3, \Delta\mathbf{V} = 3$

1) Missing transform order or scale vector control parameters

We consider three scenarios where a malicious interceptor lacks either transform order, and scale vector, or both of them. We compare the BER performance of the malicious interceptor in these three scenarios with that of the legitimate receiver. The simulation results are shown in Fig. 6.

Based on the above simulation results, it is evident that if the malicious interceptor fails to obtain all the transform order or scale vector parameters, the BER performance of the interceptor will significantly degrade, which makes it impossible for them to intercept and demodulate the communication signals as intended.

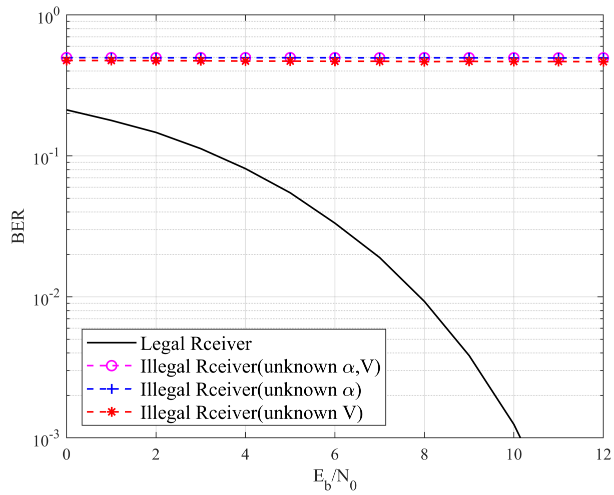

Fig. 6: BER performance of malicious interceptor and legitimate receiver under Scenario 1.

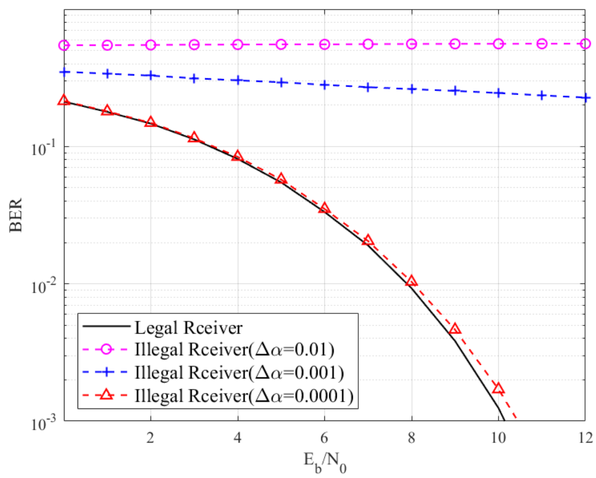

Fig. 7: BER performance of malicious interceptor and legitimate receiver under Scenario 2.

2) Completely grasping the scale vector parameters but having errors in the transform order parameters

In this section, we compare and simulate the BER performance of the malicious interceptor and the legitimate receiver under different magnitudes of the transform order error $\Delta\alpha$.The simulation results are shown in Fig. 7.

Fig.7 shows that the error magnitude of the transform order α has a crucial impact on the BER performance of the malicious interceptor when it fully grasps the scale variable parameters. The simulation reveals that when the error magnitude of α falls between 10^{-2} and 10^{-3}, the BER performance of the malicious interceptor significantly deteriorates, and communication signals cannot be intercepted and demodulated normally. However, when the error magnitude of α is 10^{-4}, the BER performance of the malicious interceptor is improved significantly and gets close to that of the

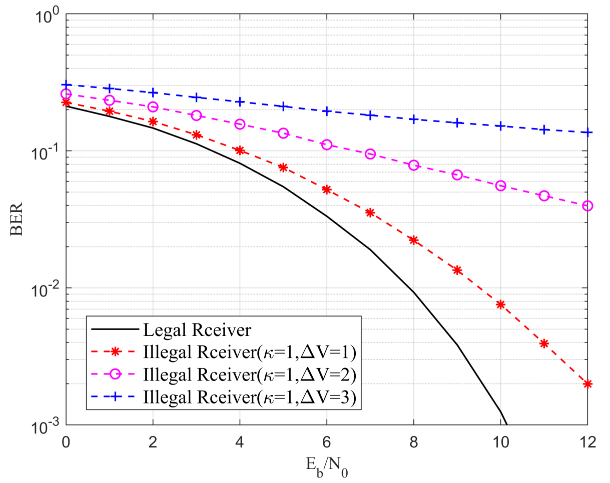

Fig. 8: BER performance of malicious interceptor and legitimate receiver under Scenario 3($\kappa = 1$)

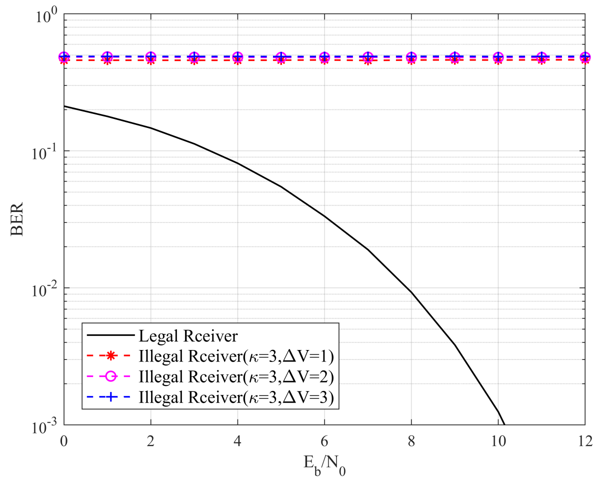

Fig. 10: BER performance of malicious interceptor and legitimate receiver under Scenario 3($\kappa = 3$)

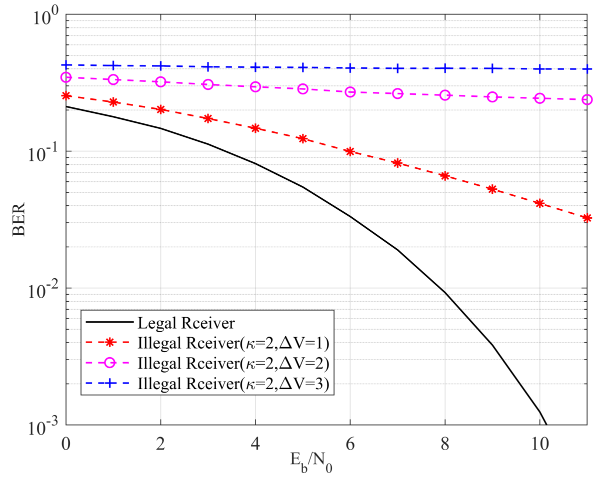

Fig. 9: BER performance of malicious interceptor and legitimate receiver under Scenario 3($\kappa = 2$)

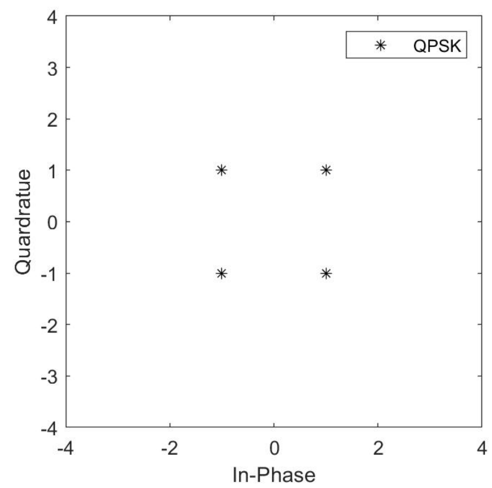

Fig. 11: Original QPSK signal

legitimate receiver. Therefore, 10^{-4} can be considered as an error magnitude boundary, and the interceptor needs to scan α at an interval of 0.001. During the entire cycle of α, the eavesdropper needs to scan a total of 4,000 times.

3) Completely grasping the transform order parameters but having errors in the scale vector parameters

In this section, we compare and simulate the BER performance of the malicious interceptor and the legitimate receiver for the number of error parameters κ and the error value $\Delta\mathbf{V}$ in the scale vector. When the number of error parameters is large, it will be similar to the state of Scenario 1. Therefore, we only consider the errors within three parameters, with error values $\Delta\mathbf{V}$ of 1, 2, and 3, respectively. The simulation results are shown in Figs. 8-10.

Based on the above simulation results, it is evident that the scale vector error significantly affects the BER of the malicious interceptor, assuming that the interceptor has complete knowledge of the transform order parameters. The BER of the interceptor is improved significantly with an increase in the number of error parameters. When the number of error parameters is 3, the performance is similar to the state where a scale vector parameter is missing in Scenario 1. However, when the number of error parameters is 1, the BER of the interceptor is relatively low, indicating some usability. Within the specified number of error parameters, the BER of the interceptor deteriorates sharply with an increase in the error value. As the scale vector $\mathbf{V}$ comprises eight parameters, it is almost impossible for the interceptor to obtain seven parameters by using the parameter scanning method, making its identification probability nearly zero. Thus, the scale vector $\mathbf{V}$ exhibits better anti-scanning performance.

D. Constellation Deception Simulation

The application of MP-WFRFT involves constellation deception. The original QPSK signal undergoes the processing by MP-WFRFT to generate a 16QAM modulated deception signal and a noise deception signal.

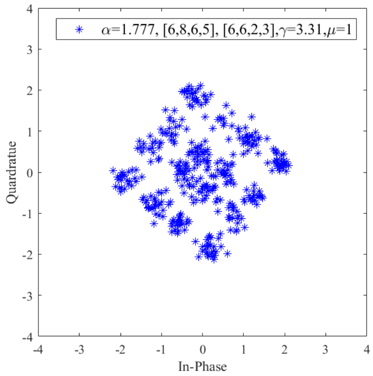

(a)

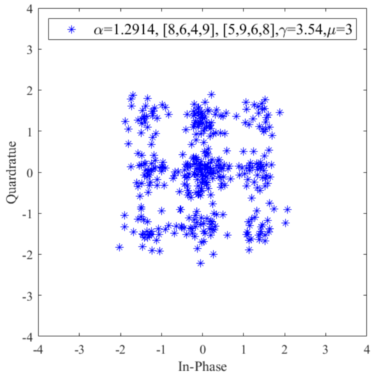

(b)

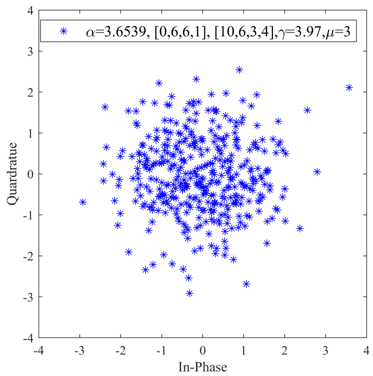

(c)

Fig. 12: (a) Random parameter set R1. (b) Random parameter set R2. (c) Random parameter set R3.

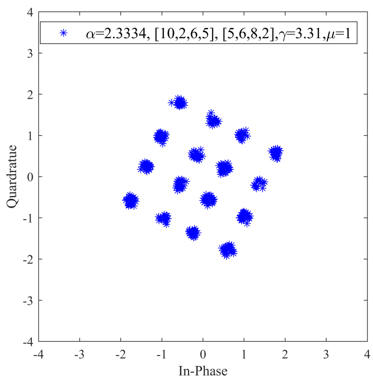

Fig. 13: Modulation deception parameter set Q1

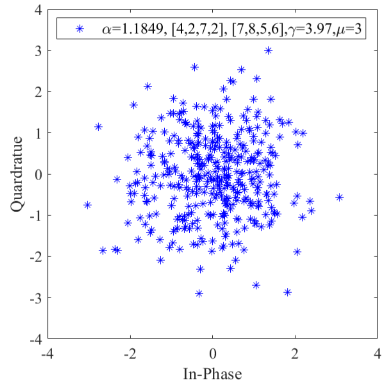

Fig. 14: Noise deception parameter set N1

TABLE II: Random Control Parameters Set

Parameters	R1	R2	R3
α	1.7770	1.2914	3.6539
$\mathfrak{M}$	[6,8,6,5]	[8,6,4,9]	[0,6,6,1]
$\mathfrak{N}$	[6,6,2,3]	[5,9,6,8]	[10,6,3,4]
W_{sc}	0.02	0.08	0.77
W_{mc}	0.98	0.92	0.23
γ	3.31	3.54	3.97
μ	1	3	3

TABLE III: The Optimal Parameters Set For Modulation Deception After Joint Optimization

Parameters	Q1
α	2.3334
$\mathfrak{M}$	[10,2,6,5]
$\mathfrak{N}$	[5,6,8,2]
W_{sc}	0^+
W_{mc}	1^-
γ	3.31
μ	1

TABLE IV: The Optimal Parameters Set For Noise Deception After Joint Optimization

Parameters	Q1
α	1.1849
$\mathfrak{M}$	[4,2,7,2]
$\mathfrak{N}$	[7,8,5,6]
W_{sc}	1^-
W_{mc}	0^+
γ	3.97
μ	3

The signal constellation diagram can intuitively judge the effect of constellation deception. We use the signal constellation diagram to compare the performance of the random control parameter set with that of the optimal control parameter set. The simulation results are presented in Figs. 11-14.

Fig. 11 displays the constellation diagram of the original QPSK modulated signal. Fig. 12(a-c) and TABLE II depict the constellation diagrams generated by random control parameter sets R1, R2, and R3. Fig. 13 shows the constellation diagram generated by the modulation deception parameter set Q1 in Table III, while Fig. 14 displays the constellation diagram generated by the noise deception parameter set N1 in Table IV. It can be found from the simulation results that the signal constellation diagram generated by the optimal parameter set is the closest to the constellation diagram characteristics of the target signal.

V. Conclusion

The PAPR suppression of the MC system is of great research significance and application value. In this work, we adopt the hybrid carrier regulating mechanism of MP-WFRFT to suppress PAPR. Due to the unitary matrix characteristics of MP-WFRFT, the BER will not deteriorate. Due to the hybrid carrier characteristics of MP-WFRFT, the system has excellent anti-scanning performance. The proposed joint optimization model for PAPR and constellation deception utilizes iterative optimization of genetic algorithm to obtain a set of control parameters with optimal PAPR and constellation deception capabilities. The simulation results suggest that the proposed method has the optimal PAPR suppression when the BER does not deteriorate, decoupling PAPR and BER. The simulation results also demonstrate that the proposed method exhibits good anti-scanning capability in various interception scenarios.

References

[1] B. Wang, Q. Si and M. Jin, "A Novel Tone Reservation Scheme Based on Deep Learning for PAPR Reduction in OFDM Systems," *IEEE Communications Letters.*, vol. 24, no. 6, pp. 1271-1274, June 2020.

[2] Y. Xia, D. Kong, Y. Xin, L. Xiao and T. Jiang, "LDPC Codes Over GF(q) With Alterable Subset for PAPR Reduction in OFDM Systems," *IEEE Communications Letters.*, vol. 26, no. 10, pp. 2262-2266, Oct. 2022.

[3] Wisam F. Al-Azzo, Borhanuddin M. Ali, Sabira Khatun, and Thabit S. Mohammed, "Tone Reservation Based on Fourier Transformed Sequence for PAPR Reduction in OFDM Systems," *Engineering Letters.*, vol. 23, no.4, pp239-244, 2015

[4] Liu X, Zhang X, Xiong J, et al. "An enhanced iterative clipping and filtering method using time-domain kernel matrix for PAPR reduction in OFDM systems," *IEEE Access.*, vol. 7, pp. 59466–59476, 2019.

[5] Liu X, Zhang X, Zhang L, et al. "PAPR reduction using iterative clipping/filtering and ADMM approaches for OFDM-based mixed-numerology systems," *IEEE Transactions on Wireless Communications.*, vol. 19, no. 4, pp. 2586–2600, 2020.

[6] Traian E. Abrudan, Stepan Kucera, and Holger Claussen, "Unitary checkerboard precoded OFDM for low-PAPR optical wireless communications," *Journal of Optical Communications and Networking.*, vol. 14, pp. 153–164, 2022.

[7] X. Da, et al. "Embedding WFRFT Signals Into TDCS for Secure Communications," *IEEE Access.*, vol. 6, pp. 54938-54951, 2018.

[8] Liang Y and Da X, "Analysis and Implementation of Constellation Precoding System Based on Multiple Parameters Weighted-type Fractional Fourier Transform," *Journal of Electronics & Information Technology.*, vol. 40, pp. 825-831, 2018.

[9] Liang Y, Da X, Xu R, et al. "Analysis on Constellation Splitting of 8PSK in MP-WFRFT-based Systems," *Advanced Engineering Sciences.*, vol. 50, pp. 179-185, 2018.

[10] F. Liu, L. Wang, J. Xie, Y. Wang and Z. Zhang, "MP-WFRFT and Chaotic Scrambling Aided Directional Modulation Technique for Physical Layer Security Enhancement," *IEEE Access.*, vol. 7, pp. 74459-74470, 2019.

[11] Q. Cheng, J. Zhu, J. Luo, "Secure spatial modulation based on dynamic multi-parameter WFRFT," *IEICE Transactions on Communications.*, vol. 101, no. 11, pp. 2304–2312, 2018.

[12] X. Wang, L. Mei, Z. Wang and X. Sha, "Enhanced Clipping and Filtering with WFRFT for PAPR Reduction in OFDM Systems," in *2019 IEEE Wireless Communications and Networking Conference (WCNC)* 2019, pp. 1–6.

[13] X. Wang, L. Mei, Z. Wang, et al. "Analysis of Weighted Fractional Fourier Transform Based Hybrid Carrier Signal Characteristics," *Journal of Shanghai Jiaotong University (Science).*, vol. 25, pp. 27–36, 2020.

[14] X. Wang, L. Mei, Z. Wang and N. Zhang, "On the probability density function of the real and imaginary parts in WFRFT signals," *China Communications.*, vol. 13, no. 9, pp. 44–52,Sept. 2016.

[15] R. Chhikara, "The inverse Gaussian distribution: theory: methodology, and applications," *CRC Press.*, vol. 95, 1988.

Yuxiao Yang received the Ph.D. degree in information and communication engineering from the Nanjing University of Aeronautics and Astronautics, Nanjing, China. He is currently an associate professor with the College of Astronautics, Nanjing University of Aeronautics and Astronautics, China. His research interests include wireless communications, covert communication, physical layer security, satellite communications, spectrum sensing.

Xiaolu Zhang received the master's degree in electronic information from Nanjing University of Aeronautics and Astronautics, Nanjing, China, in 2023. Her research interests are wireless communications, secury communication and electronic countermeasures.

Xiaobo Shen received the bachelor's degree in optoelectronic information science and engineering from Nanjing University of Aeronautics and Astronautics, in 2022. She is currently pursuing the master's degree in electronic information from the NUAA, Nanjing, China. Her research interests are wireless communications, covert communication and electronic countermeasures.